Rydberg-electron wave-packet dynamics in parallel electric and magnetic fields and evidence for stabilization

H.H. Fielding,[1,*] J. Wals,[1] W.J. van der Zande,[2] and H.B. van Linden van den Heuvell[1,2]
[1] *Van der Waals–Zeeman Laboratory, University of Amsterdam, Valckenierstraat 65, 1018 XE Amsterdam, The Netherlands*
[2] *Foundation for Fundamental Research on Matter–Institute for Atomic and Molecular Physics, Kruislaan 407, 1098 SJ, Amsterdam, The Netherlands*
(Received 7 June 1994)

The dynamics of short-lived quasibound Rydberg-electron wave packets above the classical field-ionization limit are investigated in the presence of parallel electric and magnetic fields. The observed variations in relative peak intensities in the recurrence spectra are understood both in terms of a quantum-mechanical picture and in terms of the classical electron trajectories. The linear Zeeman term causes the Rydberg wave packet to rotate around the magnetic field axis. This rotation is observed experimentally as a sinusoidal intensity modulation superimposed on the periodic structure which is attributed to motion in the angular-momentum coordinate. The diamagnetic term stabilizes the Rydberg wave packet. This stabilization is observed experimentally as an increase in the recurrence peak intensities and the observation of recurrences after longer delays (up to twice as long as in the absence of the magnetic field). Classical trajectory calculations identify the dominant closed orbits which contribute to the experimental recurrence spectra.

PACS number(s): 32.80.Rm, 03.65.Sq, 31.10.+z, 32.60.+i

I. INTRODUCTION

Time-resolved spectroscopy is the obvious tool for investigating the physics of the short-lived Rydberg states above the classical ionization limit in parallel electric and magnetic fields. Until quite recently, however, measurements of Rydberg wave packets were hampered by the poor efficiency of the conventional photoionization detection techniques which were employed. An important improvement in the efficiency of detecting Rydberg electron wave packets was the two pump pulse Ramsey interference technique which was first proposed by Noordam *et al.* [1] and demonstrated to work by Broers *et al.* [2], Christian *et al.* [3], and Jones *et al.* [4]. Following the development of this technique, electron motion in the angular momentum coordinates was investigated above the classical field-ionization limit in an external electric field, where neither frequency-resolved experiments nor conventional time-resolved photoionization detection technique would have been appropriate [5]. In addition, investigations of bound electron wave-packet dynamics in a pure Coulombic potential and in a combined Coulombic and magnetic potential have been reported in which the intrinsically high detection efficiency of this technique proved valuable [6]. Rydberg states in combined electric and magnetic fields have also received attention. The temporal evolution of a bound Rydberg wave packet in perpendicular electric and magnetic fields, using a photoionization detection technique, has been observed by Yeazell *et al.* [7]. Although there have been a number of high resolution frequency-resolved investigations of Rydberg atoms in parallel electric and magnetic fields [8–11], until now, no time-resolved experiments have been reported. Theoretical studies of Rydberg atoms in parallel electric and magnetic fields have been inspired by the fact that the hydrogen atom Hamiltonian becomes nonseparable when the diamagnetic term is included [11,12]. For example, Mao *et al.* [11] apply closed orbit theory to account for oscillations observed, in the frequency domain, near the ionization threshold in a regime where the magnetic field dominates, or is comparable to, the electric field. Rydberg states above the classical field-ionization limit in the presence of a magnetic field whose effective strength is very much less than that of the electric field have not previously received attention. This is not too surprising since one might not expect the electron dynamics to differ significantly from those in the pure electric field. However, in this work, we demonstrate that even when the ratio of the effective strengths of the electric and magnetic fields is between 10 and 100, the magnetic field stabilizes the Rydberg electron wave packet. We present experimental observations of the stabilization of Rydberg electron dynamics in rubidium above the classical field-ionization limit in parallel electric and magnetic fields. We exploit the fact that the time-resolved two-pump-pulse technique is ideally suited to the study of such short-lived states embedded in the field-ionization continuum.

II. EXPERIMENT

Most aspects of the experiment have been described in detail elsewhere [3,5], briefly: a number of Ryd-

*Present address: Department of Chemistry, King's College London, Strand, London WC2R 2LS, United Kingdom.

 ©1995 The American Physical Society

berg states of Rb (typically between 5 and 10), with, for the various experiments, principal quantum numbers in the range $n = 23$–54 depending on the laser wavelength. The Rydberg states are excited coherently from the $5s$ ground state using the frequency doubled output of a nearly bandwidth-limited, synchronously pumped, cavity-dumped, tunable picosecond dye laser (297 nm, 2.3 ps, bandwidth 7 cm^{-1}, repetition rate 3.8 MHz). The picosecond pulse is split into two equal parts at a beam splitter which is part of a Michelson interferometer type arrangement; a translation stage in one arm of the interferometer is used to delay one pulse with respect to the other and the phase difference (i.e., the *precise* delay) between the two pulses is modulated at 6 kHz by wiggling a quartz plate in the fixed delay arm of the interferometer. A Soleil-Babinet compensator sets the polarization of the light to be either parallel or perpendicular to the magnetic and electric field axes, and the light is focused into the source region of a magnetic-bottle electron-spectrometer by a 25 cm focal length quartz lens. Excitation of two identical, but delayed, electronic wave packets in Rb takes place in a constant, uniform, dc electric field (770 − 1031 V/cm) and a magnetic field which may be varied over the range 0–0.81 T. The magnitude of the magnetic field in the interaction region was measured, as a function of the current through the magnet coils, using a Hall probe. To create a uniform electric field in the interaction region, electric potentials of equal magnitude but of opposite sign were applied to two tantalum field plates (15 mm diameter with 2.5 mm diameter holes covered with coarse tungsten mesh, separated by 3.9 mm) and the nozzle of the Rb oven (2 mm below the center of the interaction region) was grounded. The electric field serves the dual purpose of providing a Stark field and directing the field-ionized Rydberg electrons to a microchannel plate.

A large number of states is excited coherently within the bandwidth of the laser excitation pulse creating a temporally localized wave packet which, at the time of its creation, is also spatially localized. The wave packet is initially created in the core region with an energy above the classical field-ionization limit and with orbital angular momentum, l, of unity. After a delay τ, ranging from 0–200 ps, during which the first wave packet has evolved in both the radial and angular momentum coordinates, a second wave packet is created. There is intereference if the first wave packet has returned to the core region and possesses predominantly p character. This interference will oscillate between being constructive and destructive at 6 kHz (the modulation frequency between the two optical pulses). Consequently, the time-dependent behavior of the wave packet can be monitored, on a picosecond timescale, by looking at the 6 kHz modulation on the total electron signal. The electron signal is passed through a bandpass filter set at the modulation frequency of 6 kHz and it can be shown that the root mean square of the filtered signal provides a direct measure of the absolute value of the time correlation function, $|\langle\psi(0)|\psi(\tau)\rangle|$ [5]. It should be pointed out that, as in Ref. [6], the signal decays with increasing delay in the experimental recurrence spectra. This decay is not attributed to the evolution of the wave packet in the time interval between the two laser pulses but can be attributed partly to a coherence loss as atoms move parallel to the laser beam over a distance comparable with a quarter of the laser wavelength; in addition, any distortion of the wave front of the laser beam results in a poorer overlap of the two pulses in the focus in the interaction region with increasing delay between the pulses.

III. RESULTS AND DISCUSSION

We present time-resolved spectra, representing the measured amplitude of the modulated final Rydberg state population, as a function of delay between the two laser excitation pulses. The electric field, F, is varied between 770 and 1031 V/cm and the magnetic field, B, from 0 to 0.81 T, for cases with the electric field vector of the laser pulse being both parallel and perpendicular to the external fields (exciting $m = 0$ and $|m| = 1$ levels respectively); the excitation energy, E, was varied from the field-ionization threshold, $E_c = -2\sqrt{F}$, up towards the zero-field ionization limit, $E_0 = 0$. The relative effective strength of the electric field to that of the magnetic field is given by $\beta = 12F/(5n^2B^2)$ [10] (F and B in a.u.) and varies from approximately 100 to 10 for $n = 23$–54. Consequently, the Rydberg electron dynamics are dominated by the electric field and, therefore, we will begin the discussion of our results with a description of the effects of a pure electric field.

A. Electron Dynamics in an Electric Field

The problem of Rydberg-electron dynamics in a strong electric field has been addressed in some detail already [5]. In our work, we present additional data from which we draw new conclusions regarding the relative peak intensities and the effects of changing the polarization of the laser excitation pulse with respect to the axis of the external electric field. A coherent superposition of Stark states is excited in the dense region of the energy spectrum above E_c which is illustrated in Fig. 1. This figure shows a Stark spectrum for hydrogen $m = 0$ levels (calculated using perturbation theory up to the fourth order [13]), the classical field-ionization limit $E_c = -1/(16n^4)$ [14] and a Gaussian laser profile (FWHM = 7 cm^{-1}) just above the saddle point.

Some typical experimental recurrence spectra are presented in Fig. 2. From the complexity of both the calculated Stark map and of previous frequency-resolved spectroscopic studies of the resonances above E_c [15,16], it might seem surprising that such a variety of energy level spacings and intensities give rise to time-resolved spectra which show such simple periodic motion. Note that energy spacings in the frequency domain, ΔE, give rise to periodic motion in time domain, $\tau = 2\pi/\Delta E$. The simplicity of the recurrence spectra can be understood from both the quantum mechanical and the classical viewpoints. A quantum-mechanical description which

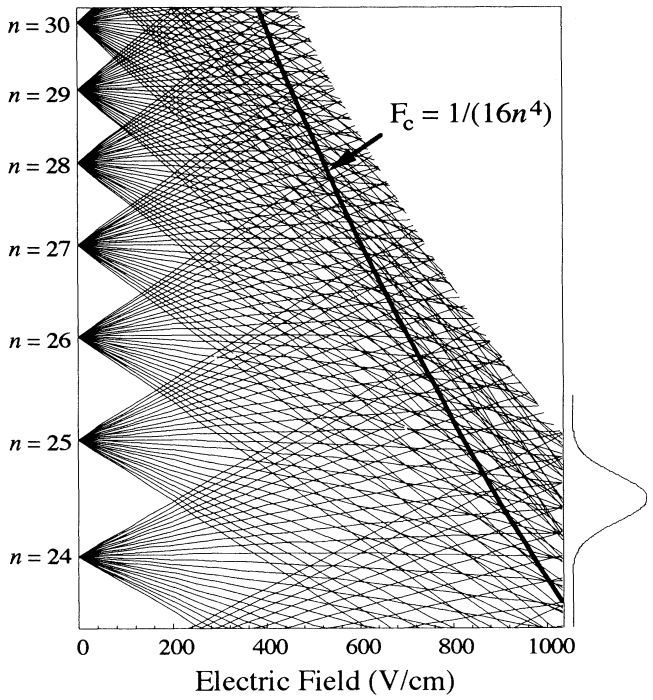

FIG. 1. Calculated Stark spectrum for hydrogen $m = 0$ levels using fourth order perturbation theory. The classical field-ionization limit, E_c, is shown by a bold line, along with a Gaussian laser profile just above E_c, with a full width at half maximum of 7 cm^{-1}, to demonstrate the large number of states contributing to the coherent superposition.

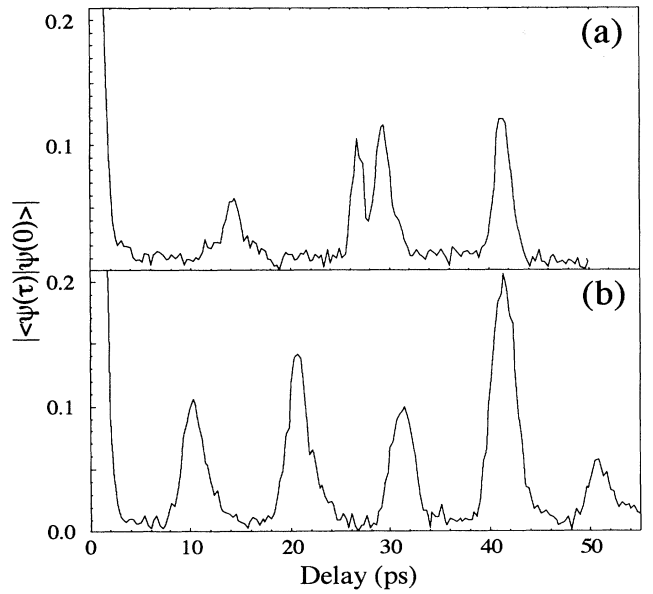

FIG. 2. Experimental recurrence spectra for excitation of Stark states with $|m| = 1$ centered around (a) $\bar{n} = 26.25$ with $F = 770$ V/cm and (b) $\bar{n} = 25.31$ with $F = 1031$ V/cm. The corresponding periods of angular electron motion, calculated using first order perturbation theory [$\tau_k = 2\pi/(3\bar{n}F)$], are (a) 12.9 ps and (b) 10.0 ps. (a) shows a double peak structure which has a splitting of 2.4 ps due to the radial motion, and (b) shows variations in the relative peak intensities.

takes into account, qualitatively, both the intensities and the field-ionization lifetimes of the parabolic eigenstates is considered first and the classical picture of closed electron orbits is discussed in Secs. III B and III C. Figure 2(a) represents a recurrence spectrum for excitation of Stark states with $|m| = 1$ around $\bar{n} = 26.25$ in an electric field of $F = 770$ V/cm, where $\bar{n}$ is the average principal quantum number in the superposition, defined by the maximum intensity of the laser excitation pulse. Figure 2(b) was recorded for excitation of $|m| = 1$ Stark states centered around $\bar{n} = 25.31$ in a larger electric field of $F = 1031$ V/cm. The period of electron motion in the angular momentum coordinate can be calculated using the first order Stark energy splittings, $\tau_k = 2\pi/\Delta E = 2\pi/(3\bar{n}F)$ [2] and is 12.9 ps for $\bar{n} = 26.25, F = 770$ V/cm and 10.0 ps for $\bar{n} = 25.31, F = 1031$ V/cm. The periods observed in the experimental spectra are 14.1 ps and 10.4 ps, respectively, and the discrepancy with the calculated values is addressed below. In Fig. 2(a), a double peak structure with a splitting of 2.4 ps is clearly apparent in the second angular recurrence. This splitting is attributed to the radial motion of the wave packet as a consequence of the excitation of more than one Stark manifold in the frequency spectrum, and so the excitation of more than one n (the calculated radial motion has a period $\tau_n = 2\pi\bar{n}^3 = 2.7$ ps). Note that peaks are observed in the recurrence spectrum when the electron returns near the core region while also possessing unit angular momentum. The single peaks in the recurrence spectra are narrower than the double peak. The variations in the widths of the angular recurrences are accounted for by the phases of the radial and angular motions. The double peak arises when the radial motion is out of phase with the angular motion and the narrower peaks arise when the two motions are in phase (since the width of the radial recurrence is much smaller than that of the angular recurrence, the wings of the angular peak are effectively cut off by being out of phase with the radial motion). In Fig. 2(b), we no longer see the double peak structure of Fig. 2(a); this is attributed to a combination of radial and angular dynamics which are always in phase with one another since the angular period (10.0 ps) is an integer multiple of the radial motion (2.5 ps). The slight asymmetry of the angular recurrence peaks suggests that the two motions are not *precisely* in phase. It is interesting to note the variations of the intensities of the angular recurrences in Fig. 2(b). These variations are attributed to interference between the variety of angular periods that are present in the coherent superposition (see Fig. 1). This statement is justified by performing a simple calculation in which the transition probability, $P(t)$, for excitation of the wave packet from the $1s$ ground state in hydrogen is calculated as a function of time, $P(t) = |\langle\Psi_{1s}(r)|r|\Psi(r,t)\rangle|^2$. The electric field, F, is 1031 V/cm and $m = 1$ states centered around $\bar{n} = 25.31$ are excited. The details of this calculation are outlined in Appendix A. Figure 3 shows the results of this calculation: if just one manifold is included in the superposition ($n = 25$), dispersion free, equally spaced recurrences all with the same intensity are observed (dotted curve). If the two adjacent Stark manifolds either side of

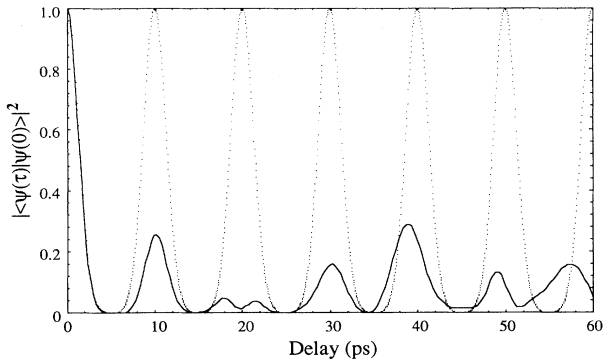

FIG. 3. Calculated recurrence spectra for exciting $m = 1$ Stark states centered around $\bar{n} = 25.31$, with a Gaussian laser profile with FWHM = 7 cm^{-1}, in an electric field of 1031 V/cm. Including only Stark states from the $n = 25$ manifold results in equally spaced, dispersion free recurrences with the same intensity (dotted curve) while including neighboring manifolds, from $n = 23$–27, demonstrates the variations in recurrence intensities and the double peak structure accounted for in terms of the interference of the different angular periods and the radial motion (solid curve).

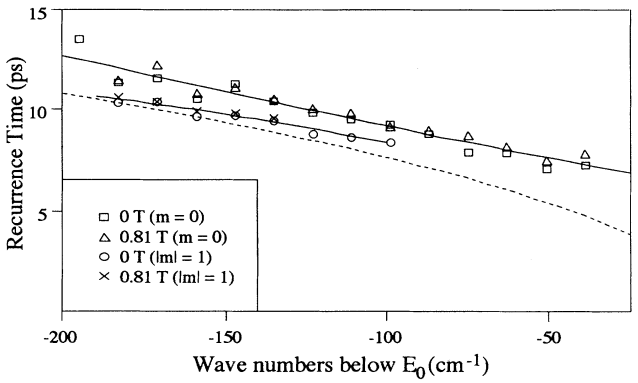

FIG. 4. Measured recurrence times for angular motion in an electric field of 1031 V/cm, for exciting states above the classical field-ionization limit centered around principal quantum numbers $\bar{n} = 23$–53, with $m = 0$ and $|m| = 1$, and in both the presence and absence of a magnetic field of 0.81 T. The scattered points are measured from experimental data and the solid curves are drawn to guide the eye. The dashed curve is the calculated angular recurrence time, $\tau_k = 2\pi/(3\bar{n}F)$.

the original one are included, i.e., $n = 23$–27, the interference between the different angular periods is observed as changes in the relative intensities of the angular recurrences and as double peak structures (full curve). Note that there is a dramatic drop in the intensity of all the recurrences. This drop is due to destructive interference both between the different angular periods and between the radial and angular periods. It should be noted that in this simple calculation, we have not included the mechanism of field ionization and, therefore, have not included the lifetimes of the Stark states which are a function of both n and k.

Not only is it worthwhile commenting on the peak intensities and profiles but it is also important to consider the recurrence periods and to be able to account for the differences between the calculated and measured recurrence times mentioned above. In Fig. 4, we present measurements of the recurrence times for the angular motion in an electric field of 1031 V/cm, for mean excitation energies $E_c = -197\ cm^{-1} < \bar{E} < E_0 = 0$ and for both $m = 0$ (parallel laser polarization) and $|m| = 1$ (perpendicular laser polarization). The dashed curve represents the closed orbit period calculated using the first order term for the Stark energy splitting within one manifold of bound k states with principal quantum number n, $\tau_k = 2\pi/(3nF)$. Figure 4 demonstrates quite clearly that the measured recurrence times for $m = 0$ are always longer than τ_k, while those measured for $|m| = 1$ roughly equal τ_k for $E \approx E_c$ but become relatively longer as E increases. This is readily explained in terms of the energy levels and intensity distribution within the coherent superposition. The transition intensity distribution within a Stark manifold of k states can be calculated using simple angular momentum algebra (the relevant $3j$ symbol is given in Appendix A) and is illustrated, for both $m = 0$ and $|m| = 1$, in Fig. 5. For $m = 0$, the intensity maxima lie at the edges of the manifold where $|k| \approx n - 1$, while for $|m| = 1$, the maximum is in the center where $k \approx 0$. In other words, for $m = 0$ the bluest and reddest Stark components, oriented predominantly along the $+z$ and $-z$ axes, respectively, dominate the electron dynamics, while for $|m| = 1$ the Stark states oriented perpendicular to the z direction, dominate. The reddest Stark states field ionize rapidly [14] and, therefore, within the $0 - 200$ ps time scale of our observations they have neglible con-

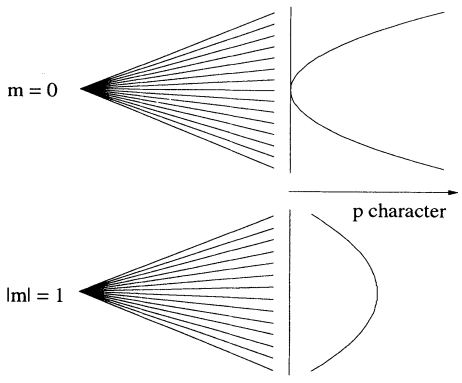

FIG. 5. Stark manifolds for excitation of $m = 0$ levels (laser polarization parallel to the electric field axis) and $|m| = 1$ levels (laser polarization perpendicular to the electric field axis). A plot of the distribution of the p character within the manifold shows that for $m = 0$ states the bluest and reddest Stark components have most p character while for the $|m| = 1$ states, the p character is localized towards the center of the manifold.

tribution to the wave-packet dynamics. Consequently, the dominant contribution for $m = 0$ states comes from the bluest Stark states which have a principal quantum number, n, which is smaller than the mean value, $\bar{n}$, corresponding to the mean laser excitation energy, $\bar{E}$. Since the angular orbit period, τ_k, is inversely proportional to n, then it can be understood that the $m = 0$ recurrence spectra will have peaks with period $\tau_k > 2\pi/(3\bar{n}F)$. For the $|m| = 1$ spectra, the wave packet is dominated by $k \approx 0$ with $n \approx \bar{n}$ and the recurrence peaks will have periods $\tau_k \approx 2\pi/(3\bar{n}F)$. As E increases above E_c, the lifetimes of all the k states decrease and only the bluest Stark states survive; as a result, the measured $|m| = 1$ orbit periods tend towards those measured for $m = 0$ until the point where there is almost no intensity in the k states which have sufficiently long lifetimes to be measurable.

B. Electron Dynamics in Parallel Electric and Magnetic Fields

In this section, we discuss the effects of the relatively small external magnetic field, of up to 0.81 T, on the electron dynamics in a large external electric field, above E_c. The Hamiltonian (in a.u.) for a spinless one-electron atom in parallel electric and magnetic fields, both directed in the z direction, is in cylindrical coordinates (ρ, z, ϕ):

$$\mathcal{H} = \mathcal{H}_0 + Fz + \frac{1}{2}mB + \frac{1}{8}B^2\rho^2 \quad , \tag{1}$$

where $\mathcal{H}_0 = p^2/2 - 1/r$ is the Hamiltonian in the absence of any external field and $r = \sqrt{z^2 + \rho^2}$. The linear Zeeman (paramagnetic) term is independent of n, while the term quadratic in B (the diamagnetic term) is proportional to n^4.

In our experiments, where the relative effective strength of the electric field is much larger than that of the magnetic field, the electric field dominates the electron wave-packet dynamics and indeed the measured angular recurrence times are independent of whether the magnetic field is present or not (see Fig. 4).

In Fig. 6, we present a series of recurrence spectra for excitation of $|m| = 1$ levels centered around $\bar{n} = 26.25$ in a fixed electric field of 821 V/cm and a magnetic field which was varied over the range $0 - 0.79$ T. The intensities of each of the spectra have been normalized on the initial peak at zero delay and are all plotted on the same vertical scale. In these recurrence spectra there is an overall sinusoidal intensity modulation superimposed on the angular motion. The frequency of the sinusoidal intensity modulation is proportional to the applied external magnetic field and, for $B = 0.79$ T, the modulation has a period of 45 ps which corresponds to an energy spacing of 0.74 cm^{-1}. This effect, which was also observed in bound Rydberg wave-packet dynamics in a combined Coulombic and magnetic potential [6], is readily understood by considering the linear Zeeman effect. The sinusoidal motion arises due to the superposition of the $|m| = 1$ wave functions which are split by the paramagnetic term in Eq. (1); the energy splitting, and hence the frequency of modulation, is proportional to the magnetic field. This can be viewed as a rotation of the charge density around the z axis with the Larmor frequency, $\omega_L = B/2$, whose projection onto the plane of polarization of the laser pulse results in a sinusoidal motion with frequency twice the Larmor frequency. For each measured magnetic field strength, this sinusoidal motion is calculated and plotted as a dotted curve in the figure. It is interesting to note that since this rotation of the charge around the field axes takes place for excitation above E_c, where the electron is only quasibound, there is a direct analogy with the cyclotron motion of a free electron in a magnetic field which gives rise to Landau resonances [18]. For $m = 0$, there is no rotation of the wave function and, consequently, no periodic intensity modulation.

Note that, as the magnetic field is increased there is an increase in the relative intensities of some recurrence peaks, most noticeably towards longer delays. In a field of 0.60 T, the fifth angular recurrence appearing after 60 ps delay is more intense than at 0 T and it also appears as a double peak. In a field of 0.46 T, the sixth and seventh recurrences, appearing between 70 and 90 ps delay, are more intense than in the absence of the magnetic

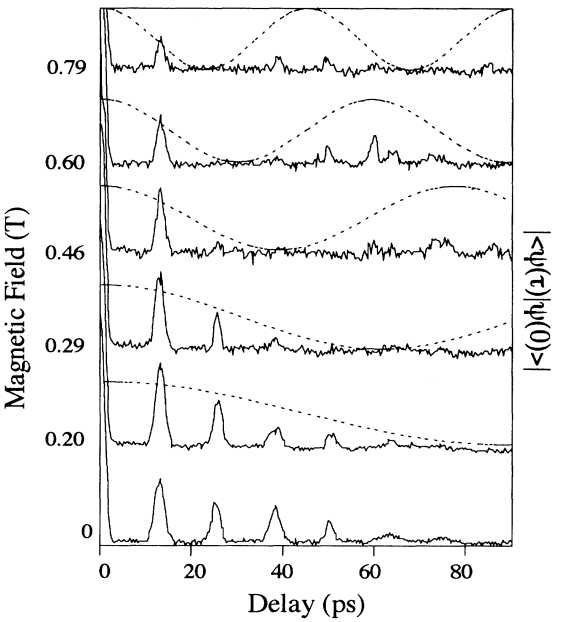

FIG. 6. A series of angular recurrence spectra for excitation of $|m| = 1$ levels centered around $\bar{n} = 26.25$ in a fixed electric field of 821 V/cm. The strength of the magnetic field is varied from 0 to 0.79 T and is labeled on the vertical axis. The overall sinusoidal intensity modulation which can be observed in the experimental spectra is emphasized by the calculated, dashed, sinusoidal curves which have periods which are twice the Larmor frequency, $\omega_L = B/2$, arising as a result of a rotation of the Rydberg wave function around the magnetic field axis.

field. From the quantum-mechanical viewpoint, the energy level structure and the transition line intensities and shapes are perturbed by the introduction of the magnetic field through the diamagnetic term in the Hamiltonian.

The diamagnetic term has the effect of mixing the zero-field angular momentum states with the selection rule $\Delta l = 0$ and ± 2, compared to the electric field which mixes states with $\Delta l = \pm 1$; obviously, this will influence the nature of the interference between the variety of angular periods contributing to the wave-packet dynamics. From a classical viewpoint, the peaks in the recurrence spectrum represent closed orbits and they appear at delays which are equal to, or multiples of, the periods of the closed orbits. These closed orbits are linked to an oscillatory motion in the angular-momentum coordinate which can be demonstrated by performing a classical trajectory calculation. The electron trajectory is followed in terms of the classical parameters r (the distance from the nucleus) and l (the orbital angular momentum). Figure 7 shows plots of $r(t)$ and $l(t)$, where $l(t) = |\mathbf{r}(t) \times \mathbf{p}(t)|$. It is clear from this figure that the experimental orbit period is linked to the period of oscillation in the angular momentum. The radial oscillation is much faster and there is an overall modulation in the distance of closest approach to the core which reflects the oscillation in angular momentum. It is apparent that a double quantum beat will be observed when both the distance from the core is small and the angular momentum is low. The intensities of the peaks in the recurrence spectrum are a measure of the stabilities of the closed orbits [19]. Thus, it is evident from the experiment that adding a magnetic field has the effect of stabilizing the closed orbits contributing to the recurrence spectrum. This stabilization has already been considered in a theoretical paper [11], but has not been observed experimentally until now. The fact that after longer delays the recurrence peaks are more intense in the presence of the magnetic field is the same as saying that the Rydberg atom is stabilized against field ionization. This stabilization is only obvious in Fig. 6 near the maxima of the superimposed sinusoidal intensity modulation, that is when the charge density which is rotating around the magnetic field axis is aligned with the polarized laser field.

In Fig. 8, we present spectra measured for excitation of $m = 0$ states centered around $\bar{n} = 24.47$ in an electric field of 1031 V/cm, both in the absence of a magnetic field and in the presence of a field of 0.81 T. Here, there is no sinusoidal modulation to obscure the effects of the stabilization in the magnetic field. After the first recurrence, all the peaks become more intense and, in fact, when the magnetic field is present peaks are observed after delays which are twice as long as in its absence. The fourth recurrence is barely visible in the absence of a magnetic field but becomes very intense when the field is turned

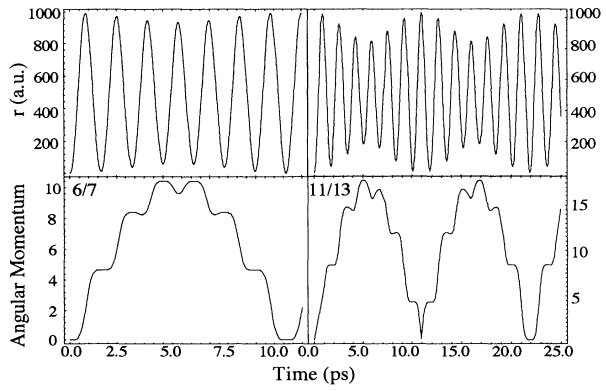

FIG. 7. Plots of $r(t)$ (upper pictures) and $l(t)$ (lower pictures) for the 6/7 and the 11/13 closed orbits which are drawn in Fig. 8. Note that the motions in the angular-momentum coordinate have periods of 11.0 ps and 21.6 ps for the 6/7 and 11/13 orbits, respectively. $r(t)$ and $l(t) = |\mathbf{r}(t) \times \mathbf{p}(t)|$ are deduced using the classical trajectory calculation which is described in Appendix B for $F = 1031$ V/cm, $B = 0.81$ T, and $\bar{n} = 24.47$.

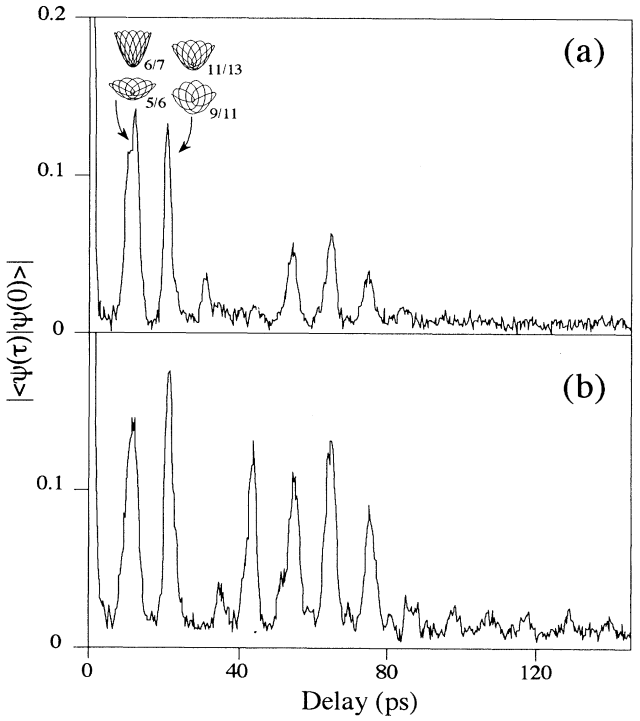

FIG. 8. Recurrence spectra for excitation of $m = 0$ states, centered around $\bar{n} = 24.47$ in an electric field of 1031 V/cm and magnetic fields of (a) 0 T and (b) 0.81 T. The period of the angular recurrences is determined by the electric field but the magnetic field is seen to have a stabilizing influence on the classical electron trajectory. All the recurrence peaks are more intense and recurrences are visible after a longer delay ($\tau > 80$ ps) in the presence of the magnetic field. A particularly interesting feature is the appearance, in the magnetic field, of the large fourth recurrence which is barely visible in the absence of the magnetic field. The dominant closed orbits are illustrated above the first two recurrence peaks to which they correspond.

TABLE I. A list of the number of recurrence peaks observed in the experimental recurrence spectra for excitation of states with both $m = 0$ and $|m| = 1$ in the presence of a magnetic field of 0 T or 0.81 T as a function of the fraction of the excitation energy above the saddle point. Note that the stabilizing influence of the magnetic field (given qualitatively as a fraction of the peaks with and without the B field) decreases with increasing energy above the saddle point.

$(E_c - E)/E_c$	$\|m\|$	No. recurrences ($B = 0$ T)	No. recurrences ($B = 0.81$ T)
0.111	0	4	4
0.111	1	6	7
0.079	1	5	7
0.074	0	4	6
0.074	1	6	8
0.049	0	8	13
0.049	1	5	8

on. In addition, after a delay of approximately 50 ps, the magnetic field causes a number of small, peaks to become visible which have recurrence times which are different to those of the dominant peaks. The number of recurrence peaks (possessing the dominant angular period) that are visible in the recurrence spectra in the presence of the magnetic field, compared to the number that are visible in its absence, provides a qualitative measure of the degree of stabilization against field ionization. This stabilization is most evident when a wave packet is created just above the saddle point, E_c, so that the states in the superposition are sufficiently long lived on our picosecond timescale. Table I lists the number of recurrence peaks observed both in the absence and the presence of a magnetic field of 0.81 T for excitation of $m = 0$ levels as a function of the fraction of the excitation energy above the saddle point, $(E_c - E)/E_c$.

C. Closed Orbit Calculations

In order to gain deeper insight into the classical picture of a quasibound electron moving in parallel electric and magnetic fields, we have performed classical trajectory calculations. With the aid of these calculations, we are able to identify the dominant closed orbits in the experimental spectra and to link these closed orbits with an oscillatory motion in the angular-momentum coordinate. The details of the calculations are described in Appendix B. The procedure is to launch an electron from the origin at an angle θ to the $-z$ axis, using cylindrical coordinates (ρ, z), and to determine whether the trajectory is closed, that is whether it returns to the origin at some later time. The stability of the closed orbit is a measure of the sensitivity of the degree of closure to the initial launching angle. It is worthwhile to note a number of general results of these calculations. There is only one *stable* closed orbit in this system which is the straight line orbit along the $+z$ axis ($\theta = 180°$) [20]. This can be compared directly with the quantum-mechanical description of excitation of the long-lived, blue shifted Stark states whose wave functions are localized towards the uphill ($+z$) side of the potential. When $E \geq 0$, this stable orbit is the only closed orbit of the system. As E decreases, other closed orbits with different launching angles bifurcate out of the stable orbit and close to E_c there will be a huge number of closed orbits. At a particular energy, $E_c < E < E_0$, there is a critical angle, $\theta_{\rm crit}$, below which there are no closed orbits, that is to say that an electron launched at $\theta < \theta_{\rm crit}$ will escape over the saddle point and field ionize. In the hydrogen atom (for which our calculations apply) the closed orbits, with $\theta > \theta_{\rm crit}$, are stable against field ionization; however, in any other atom such as rubidium, the effect of the finite size of the ion core is to cause a precession of the closed orbit in a plane containing the z axis, so that the electron will eventually escape over the saddlepoint and field ionize. In semiparabolic coordinates (u, v), in which the Hamiltonian is separable for the limiting case that $B \to 0$, this critical angle can be represented in the form of a separatrix in a plot

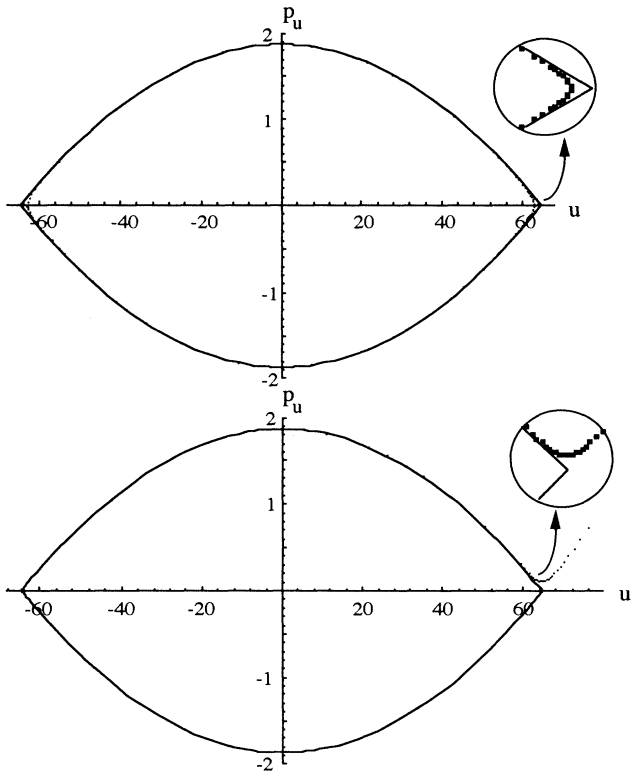

FIG. 9. Results of the classical trajectory calculation are presented in this figure to demonstrate quantitatively that the magnetic field stabilizes the atom against field ionization. (a) represents a plot of the separatrix (solid line) for $F = 1031$ V/cm, $B = 0$ T, and $\bar{n} = 24.47$, corresponding to $\theta_{\rm crit} = 42.3741°$. The dashed line represents a more stable orbit when an electron is launched at the same angle in a B field of 0.81 T. (b) represents a plot of the separatrix (solid line) for $F = 1031$ V/cm, $B = 0.81$ T and $\bar{n} = 24.47$, corresponding to $\theta_{\rm crit} = 41.9260°$. The dashed line represents an unstable trajectory of an electron which is field ionized after being launched at the same angle in a B field of 0 T.

of p_u against u (the surface of section), where p_u is the momentum along the u coordinate [20]. The separatrix condition is that the energy in the u coordinate equals the maximum of the potential energy associated with the u motion. Thus, the separatrix defines the boundary between orbits which are bound to the atom forever (inside the separatrix) and those that escape (outside the separatrix). Figure 9(a) shows a plot of the separatrix (solid line) when $F = 1031$ V/cm, $B = 0$ T and $\bar{n} = 24.47$ corresponding to a launching angle $\theta_{\rm crit} = 42.3714°$. If the magnetic field is turned on, $B = 0.81$ T, then this same angle launches the electron into a more stable orbit inside the separatrix (dotted line). Figure 9(b) shows a plot of the separatrix (solid line) when $F = 1031$ V/cm, $B = 0.81$ T and $\bar{n} = 24.47$ corresponding to a launching angle of $\theta_{\rm crit} = 41.9260°$. Turning off the magnetic field, $B = 0$ T, results in field ionization as the electron follows a trajectory outside the separatrix. The insets in the figure show enlarged portions of the orbits for clarity.

In the case $F = 1031$ V/cm, $\bar{n} = 24.47$, and $B = 0$ or 0.81 T, a large number of closed orbits contribute to the recurrence spectrum. The four dominant closed orbits are listed in Table II, together with their launching angles and periods in magnetic fields of both 0 T and 0.81 T. The labels u/v represent the number of periods in the u and v coordinates before closure. The orbits are drawn in cylindrical coordinates (ρ, z) and presented in Fig. 8, above the first two recurrence peaks to which they correspond. The 6/7 and 5/6 orbits will contribute to all the peaks in the recurrence spectrum (periods 10.95 and 10.62 ps and multiples of these) and the 11/13 and 9/11 orbits will contribute to all the even-numbered recurrences (periods 21.62 and 20.89 ps and multiples of these). From this picture it follows that the dominant peaks in the recurrence spectrum will have line profiles and intensities which depend both on the amplitude and the phase of the contributing closed orbits. Note that, the amplitudes of the peaks in the experimental recurrence spectrum also depend on the precession of the closed orbits in the plane containing the z axis. The additional small recurrence peaks that appear between the dominant peaks in the case where the magnetic field is present arise from the stabilization of closed orbits with periods which are not multiples of the dominant closed-orbit periods.

TABLE II. A list of the four dominant closed orbits observed in Fig. 8, together with their launching angles and periods. The orbits were calculated using the classical trajectory calculation described in Appendix B.

Orbit (u/v)	$B = 0$ T		$B = 0.81$ T	
	$\theta(°)$	τ (ps)	$\theta(°)$	τ (ps)
6/7	77.1478	10.95	75.8150	11.01
11/13	67.2125	21.62	66.4803	21.68
5/6	60.0740	10.62	59.5503	10.65
9/11	53.9903	20.89	54.5884	20.92

IV. CONCLUSION

We have presented measurements of quasi bound Rydberg electron dynamics above the classical field ionization limit in parallel electric and magnetic fields. The dominant closed orbits contributing to the experimental recurrence spectra have been identified with the aid of classical trajectory calculations and it has been shown that these closed orbits correspond to a periodic motion in the angular-momentum coordinate. The paramagnetic term in the Hamiltonian causes the wave packet to rotate around the magnetic field axis with the Larmor frequency and this motion was observed in the experimental recurrence spectra as a sinusoidal intensity modulation superimposed on the regular periodic structure arising from the motion in the angular-momentum coordinate. The diamagnetic term in the Hamiltonian has the effect of stabilizing the Rydberg wave packet. This stabilization was observed experimentally as an increase in the recurrence peak intensities and also in the presence of recurrence peaks after longer delays. Together with classical trajectory calculations, these observations provide evidence that the individual closed orbits are stabilized in the magnetic field and that the Rydberg atom is also stabilized against field ionization. It is hoped that this work will stimulate more interest in Rydberg electron dynamics in external fields where the diamagnetic term is important, but not necessarily dominating the electron dynamics. In addition, it would be of interest to extend the calculations for the hydrogen atom to the actual atomic systems that are being used in the experiments.

ACKNOWLEDGMENTS

The authors gratefully acknowledge B. Broers and H.G. Muller for helpful discussions and also thank J.F. Christian and L.C. Snoek for their help with the setting up of the experiment. The work in this paper is part of the research program of the "Stichting voor Fundamenteel Onderzoek van de Materie" (Foundation for Fundamental Research on Matter) and was made possible by financial support from the "Nederlandse Organisatie voor Wetenschappelijk Onderzoek" (Netherlands Organization for the Advancement of Research). H.H.F. would like to thank the Royal Commision for the exhibition of 1851 (U.K.) for financial support.

APPENDIX A: TIME-DEPENDENT TRANSITION PROBABILITY

The time-dependent transition probability can be calculated using

$$P(t) = \left| \sum_n R_n \sum_k \begin{pmatrix} (n-1)/2 & (n-1)/2 & 1 \\ (m-k)/2 & (m+k)/2 & -m \end{pmatrix}^2 A_{nkm}\, e^{i\omega_{nkm}t} \right|^2. \quad \text{(A1)}$$

The overlap integral, $R_n = \int_0^\infty R_{np} r R_{1s} dr$, is integrated numerically using the hydrogenic wave functions R_{nl}. The $3j$ symbol represents the projection of the orbital angular-momentum states, $|nlm\rangle$ (which are no longer eigenstates of the system), onto the parabolic eigenstates, $|nkm\rangle$ [18]. A_{nkm} is proportional to the Gaussian envelope of the exciting laser pulse. The Stark energy levels, ω_{nkm}, in the phase factor, are calculated using fourth order perturbation theory.

APPENDIX B: CLOSED-ORBIT CALCUATION

Following the convrntion in Ref. [21], omitting the constant Zeeman term and setting $m = 0$ in the Hamiltonian [Eq. (1)], we choose parabolic coordinates (u, v) which are related to the cylindrical coordinates (ρ, z) by the following transformations:

$$\begin{aligned} \rho &= uv, & p_\rho &= \frac{1}{u^2+v^2}(vp_u + up_v), \\ z &= \tfrac{1}{2}(v^2-u^2), & p_z &= \frac{1}{u^2+v^2}(-up_u + vp_v). \end{aligned} \tag{B1}$$

We then introduce the regularized Hamiltonian

$$\mathcal{H}^{\rm reg} = (u^2+v^2)(\mathcal{H} - E) + 2, \tag{B2}$$

in order to remove the singularity at the origin. In the case of zero magnetic field, this regularized Hamiltonian is separable into two uncoupled equations of motion in the u and v coordinates. We then integrate the Hamilton-Jacobi equations of motion [22] numerically:

$$\begin{aligned} -\dot{p}_u(t) &= -2Eu(t) - 2Fu(t)^3 \\ &\quad + \frac{1}{2}B^2u(t)^3v(t)^2 + \frac{1}{4}B^2u(t)v(t)^4, \\ -\dot{p}_v(t) &= -2Ev(t) - 2Fv(t)^3 \\ &\quad + \frac{1}{2}B^2u(t)^2v(t)^3 + \frac{1}{4}B^2u(t)^4v(t), \end{aligned} \tag{B3}$$

where E is the field-free binding energy and

$$\begin{aligned} u(0) &= 0, & p_u(0) &= 2\cos(\theta/2), \\ v(0) &= 0, & p_v(0) &= 2\sin(\theta/2), \end{aligned} \tag{B4}$$

where θ is the firing angle in the (ρ, z) plane. After solving these equations of motion we transform back to cylindrical coordinates since it is easier to visualize the electron trajectory when it is plotted in cylindrical coordinates.

The period of the orbits in real time, $T_{\rm real}$, can be calculated using the relation

$$T_{\rm real} = \int_0^{T_{\rm reg}} r(t)dt\ , \tag{B5}$$

where $T_{\rm reg}$ is the orbit time in regularized units and $r(t) = u(t)^2 + v(t)^2$.

[1] L.D. Noordam, D.I. Duncan, and T.F. Gallagher, Phys. Rev. A **45**, 4734 (1992)

[2] B. Broers, J.F. Christian, J.H. Hoogeraad, W.J. van der Zande, H.B. van Linden van den Heuvell, and L.D. Noordam, Phys. Rev. Lett. **71**, 344 (1993).

[3] J.F. Christian, B. Broers, J.H. Hoogenraad, W.J. van der Zande, and L.D. Noordam, Opt. Commun. **103**, 79 (1993).

[4] R.R. Jones, C.S. Raman, D.W. Schumacher, and P.H. Buchsbaum, Phys. Rev. Lett. **16**, 2575 (1993).

[5] B. Broers, J.F. Christian, and H.B. van Linden van den Heuvell, Phys. Rev. A **49**, 2498 (1994).

[6] J. Wals, H.H. Fielding, J.F. Christian, L.C. Snoek, W.J. van der Zande, and H.B. van Linden van den Heuvell, Phys. Rev. Lett. **72**, 3783 (1994).

[7] J.A. Yeazell, G. Raithel, L. Marmet, H. Held, and H. Walther, Phys. Rev. Lett. **70**, 2884 (1993).

[8] P. Cacciani, S. Liberman, E. Luc-Koenig, J. Pinard, and C. Thomas, J. Phys. B **21**, 3475 (1988).

[9] P. Cacciani, C. Delsart, E. Luc-Koenig, and J. Pinard, J. Phys. B **25**, 1991 (1992).

[10] T. van der Veldt, W. Vassen, and W. Hogervorst, J. Phys. B **26**, 1945 (1993).

[11] J.-M. Mao, K.A. Rapelje, S.J. Blodgett-Ford, J.B. Delos, A. Konig, and H. Rinneberg, Phys. Rev. A **48**, 2177 (1993).

[12] M.A. Iken, F. Borondo, R.M. Benito, and T. Uzer, Phys. Rev. A **49**, 2734 (1994).

[13] M.L. Zimmerman, M.G. Littman, M.M. Kash, and D. Kleppner, Phys. Rev. A **20**, 2251 (1979).

[14] T.F. Gallagher, Rep. Prog. Phys. **51**, 143 (1988).

[15] R.R. Freeman, N.P. Economou, G.C. Bjorkland, and K.T. Lu, Phys. Rev. Lett. **21**, 1463 (1978).

[16] R.R. Freeman and N.P. Economou, Phys. Rev. A **20**, 2356 (1979).

[17] H.A. Bethe and E.E. Salpeter, *Quantum Mechanics of One- and Two-Electron Atoms* (Plenum, New York, 1977).

[18] W.R.S. Garton and F.S. Tomkins, Astrophys. J. **158**, 839 (1969).

[19] D. Wintgen, Phys. Rev. Lett. **58**, 1589 (1987).

[20] J. Gao and J.B. Delos, Phys. Rev. A **49**, 869 (1994).

[21] H. Hasegawa, M. Robnik, and G. Wunner, Prog. Theor. Phys. Suppl. **98**, 198 (1989).

[22] H. Goldstein, *Classical Mechanics* (Addison-Wesley, Cambridge, MA, 1950).